Micromachined Devices and Components, Proceedings of the SPIE, Vol 2882, Austin, TX, Oct 14-15, 1996.

Release-etch modeling for complex surface micromachined structures

W.P. Eaton* and J.H. Smith
Integrated Micromechanics, Microsensors, & CMOS Technologies Department
R.L. Jarecki
Advanced Technologies for Sub 0.35 µm Processes Department
Sandia National Laboratories
Albuquerque, NM 87185-1080

Keywords: release etch, surface micromachining

ABSTRACT

A release etch model for etching sacrificial oxides in aqueous HF solutions is presented. This model is an extension of work done by Monk *et. al.* and Liu *et. al.* The model is inherently one dimensional, but can be used to model the etching of complex three dimensional parts. Solutions and boundary conditions are presented for a number of geometries.

1. INTRODUCTION

Knowledge of release-etch kinetics is essential for designing manufacturing processes for large surface micromachined structures such as sealed diaphragms and cavities and flow channels. For these structures, etch ports can be on the top or the sides (e.g Figure 1(f,g)). Using top etch ports is attractive since diffusion limitations from long lateral etch paths can be eased. However, sealing these structures poses problems since the etch ports are generally lithographically defined, requiring relatively large holes. As a result, thicker film depositions are required to provide a seal, and the possibility of unwanted material deposition inside the cavity exists. Side etch ports, on the other hand, have heights controlled by film thicknesses or etch depths, which can have dimensions smaller than lithographic feature sizes. Because of this feature, sealing these structures is easier, but at the expense of longer etch times. Long etch times are undesirable from a manufacturing point of view for two reasons: (1) they decrease device throughput through a fabrication facility, thereby raising cost of manufacture and (2) they can potentially decrease device reliability due to etch selectivity problems.

For etching structures using either side or top etch ports, understanding the etch behavior for a given geometry can be essential to the successful fabrication of a micromachined device. In this work, a simple one dimensional model is presented which describes the etching of complex three-dimensional parts. These parts are shown in Figure 1. Etch kinetics of the simplest etch structure, the rectangular etch port, have been presented in the literature [1,2], and are repeated in part in this work for completeness.

2. THEORETICAL FOUNDATIONS

Modeling of release etching in this work is based upon finding relationships among flux, concentration, and etch rate. Figure 2 illustrates the conventions of the model, where $d(t)$ is the etch front position as a function of etch time. C_b and $C(d)$ are the bulk and surface concentrations of HF, respectively. $C(x,t)$ is the concentration of the solution anywhere in the etch cavity at a given time. As the notation implies, concentration is not explicitly calculated as a function of time, but rather a quasistatic approximation is used.

For etching oxides in aqueous HF solutions, the presumed overall reaction is

$$6HF + SiO_2 \rightarrow H_2SiF_6 + 2H_20 \quad (1)$$

The actual reaction path is known to be more complex[1,3]. For a stoichiometric reaction

* Under contract from the Center for High Technology Materials, U. of New Mexico, Albuquerque, NM 87131.

Variable	units	**description**
α	[cm³/mole]	proportionality constant
A	[mole/cm²]	constant of integration
A_1	[mole/cm²]	constant of integration in region 1
A_2	[mole/cm²]	constant of integration in region 2
A_3	[mole/cm²]	constant of integration in region 3
B	[mole/liter]	constant of integration
C	[mole/liter]	concentration of HF
C_0	[mole/liter]	concentration at region 1/region 2 boundary
C_1	[mole/liter]	concentration in region 1
C_2	[mole/liter]	concentration in region 2
C_3	[mole/liter]	concentration in region 3
C_b	[mole/liter]	bulk etchant concentration
C_w	[mole/liter]	concentration at $\delta=r_{bp}$
d	[µm]	position of etch fron at any time t
D	[cm²/sec]	diffusivity of HF in water
d_1	[µm]	width of rectangular etch port *1*
d_2	[µm]	width of rectangular etch port *2*
d_{bp}	[µm]	"break point" radius at which all bubbles join
f	–	angle determined by number of etch ports
γ_b	–	geometrical constant
g_b	[µm]	geometrical constant
h_1	[µm]	height of rectangular etch port *1*
h_2	[µm]	height of rectangular etch port *2*
J_n	[mole/ cm²·sec]	flux of species n
k_2	[cm⁴/ mole·sec]	second order etch rate coefficient
k_l	[cm/sec]	first order etch rate coefficient
L_1	[µm]	length of rectangular etch port *1*
L_2	[µm]	length of rectangular etch port *2*
MW_n	g/mole	molecular weight of species n
q	–	angle swept by etch front as etch progresses
r	[µm]	radial coordinate
r_0	[µm]	arbitrary radius above which bubble solution is valid
R_0	[µm]	radius of circular structure
t	[min]	time
t_1	[min]	etch time in region 1
t_2	[min]	etch time in region 2
u	[µm/min]	back flow velocity of etch products
x	[µm]	linear coordinate

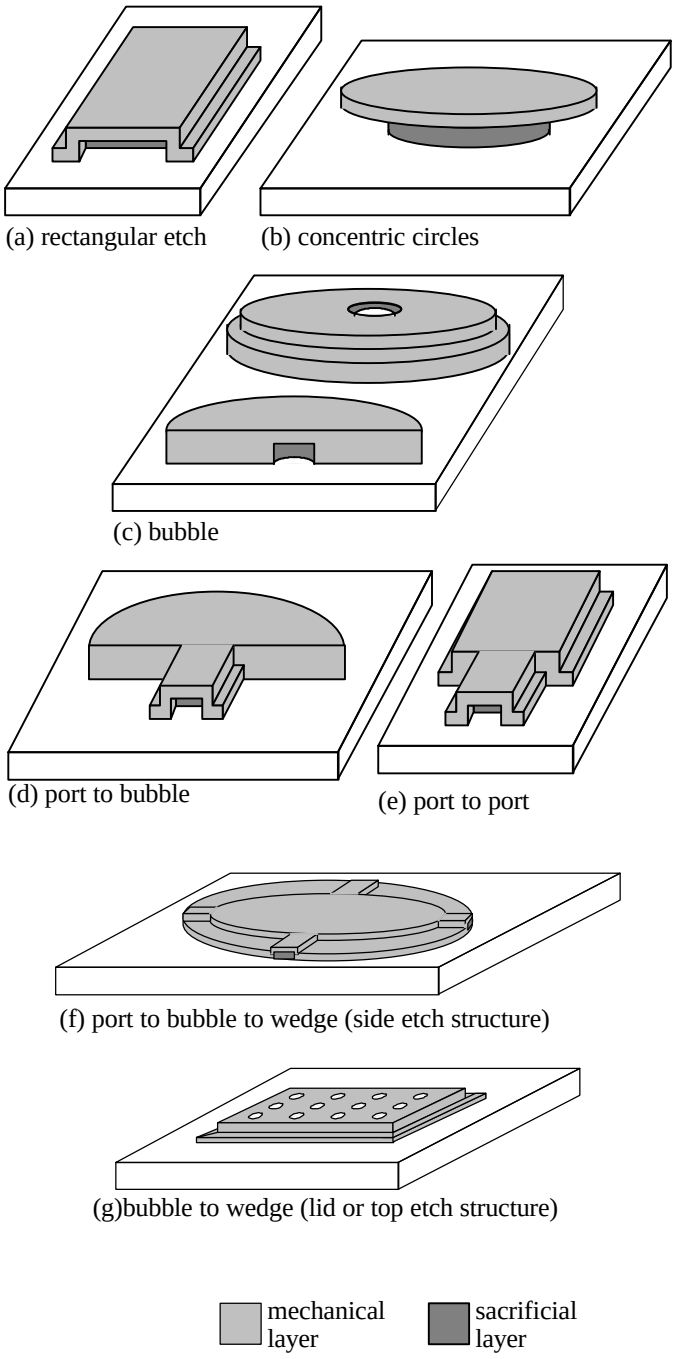

Figure 1. Possible geometric etch structures. Simple structure (a-c)are shown at top. More complex structures (d-g), shown below, are formed by combining simple structures.

$$J_{SiO_2} = \frac{1}{6} J_{HF} \tag{2}$$

Where J_{SiO_2} and J_{HF} represent the fluxes corresponding to the removal of oxide at the etch front and transport of aqueous HF to the etch front, respectively. The oxide etch front velocity is proportional to J_{SiO_2}(reference 4).

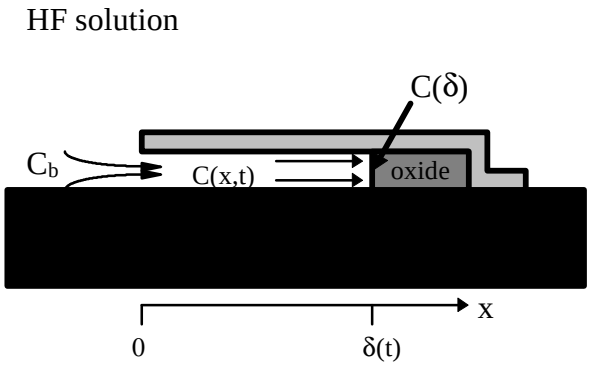

Figure 2. Conventions for coordinates and concentrations of wet etch model. After refs 1 and 2.

$$\frac{d\delta}{dt} = J_{SiO_2}\frac{MW_{SiO_2}}{\rho_{SiO_2}} \tag{3}$$

where MW_{SiO_2} and ρ_{SiO_2} are the molecular weight and mass volume density of the oxide, which are 60 [g/mole] and 2.1 [g/cm³] for pure SiO_2. Doped glasses should have similar values. It is preferable to account for only one species, namely HF. To this end, Equations 2 and 3 are combined to yield

$$\frac{d\delta}{dt} = (\alpha J_{HF})\Big|_{x=\delta} \qquad \alpha = \frac{1}{6}\frac{MW_{SiO_2}}{\rho_{SiO_2}} \tag{4}$$

Fick's first law is now invoked

$$J_{HF} = -D(\nabla C) \tag{5}$$

where D is the diffusion constant of HF, which has been measured to vary from $3.1\cdot10^{-5}$ cm^2/sec for infinite dilution to $8.8\cdot10^{-6}$ cm^2/sec for solutions of HF, H_2SiF_6, and water[3]. The flux is also assumed to take many empirical forms such as

$$J_{HF} = f(C) = \begin{cases} k_1 C \\ k_2 C^2 \\ k_1 C + k_2 C^2 \\ kC^n \end{cases} \tag{6}$$

here the $f(C)$ on the RHS represent only a few of the possible functional forms. Many of these have been examined by Monk *et al* [3,4,5]. According to Tai *et al* and Liu *et al*[1,2] , $J_{HF}=k_1C+k_2C^2$ is a good empirical choice for the functional form of the etchant, and these kinetics are used in this work. There are several reasons for using such an empirical form:

- It describes the behavior of a wide range of concentration of etching solutions[1,2].
- HF:$H_2$0:Si0$_2$ reactions are more complex than indicated by Equation 1 [1,3]
- The diffusivity, D, of HF is concentration dependent and therefore is expected to vary both spatially along a given etch channel and temporally, as a release etch progresses.
- Doped glasses have different etch rates, and possibly different etch mechanisms, than their undoped counterparts[1,3].

First order kinetics often lead to analytical solutions, and hence can be useful for predicting general behavior. Second order kinetics generally fit data better than first order kinetics, however analytical solutions are rarer; numerical integration is often required. Numerical integrations can be performed with commercial mathematical software such as Mathematica™ [6], Maple V™ [7], or MathCAD™ [8].

By the above three equations, the etch front velocity, $d\delta/dt$, can be expressed as a function of concentration. To arrive at a form for the concentration, the equation of continuity or mass balance is considered

$$u\nabla C + \dot{C} = D\nabla^2 C \qquad C\Big|_{x=0;\ all\ t} = C_b$$

$$C\Big|_{x=\delta;\ all\ t} = C(\delta) \qquad C\Big|_{all\ x;\ t=0} = C_b \qquad J_{HF} = -D\left.\frac{\partial C}{\partial x}\right|_{x=\delta} = f(C)\Big|_{x=\delta} \tag{7}$$

Where u and $\dot{C}$ are the flow velocity of the reactants and partial derivative of concentration with respect to time, respectively. C_b is the bulk concentration of HF. In general it is very difficult to solve Equation 7 explicitly. It has been demonstrated that for etching PSG, the convective term in Equation 7, ($u\tilde{N}C$), can be neglected compared with $D\tilde{N}^2C$ (reference 1). Furthermore it is assumed that this system can be considered quasistatic. That is, the instantaneous change of concentration with time is presumed to be small, i.e.

$$\dot{C} << D\tilde{N}^2C \tag{8}$$

Thus Equation 7 is simplified to become

$$D\tilde{N}^2C=0 \tag{9}$$

Which is Poisson's equation. The quaststatic approximation is used for mathematically tractability and is commonly used in heat and mass transfer problems .

For one dimensional linear and radial systems Equation 9 becomes

$$\begin{aligned} \frac{\P^2C}{\P x^2} &= 0 \\ \frac{1}{r}\frac{\P}{\P r}\left(r\frac{\P C}{\P r}\right) &= 0 \end{aligned} \tag{10}$$

and has general solutions

$$\begin{aligned} C(x) &= Ax + B \\ C(r) &= A\ln r + B \end{aligned} \tag{11}$$

For the linear case, a boundary condition of $C(0) = C_b$ is usually chosen. For the radial case, $C(0)$ is undefined. Therefore an arbitrarily small radius r_0 is chosen so that the boundary condition becomes $C(r_0) = C_b$. Therefore Equations 11 become

$$\begin{aligned} C(x) &= Ax + C_b \\ C(r) &= A\ln\left(\frac{r}{r_0}\right) + C_b \end{aligned} \tag{12}$$

All of the above equations, along with additional boundary conditions, form a framework for solving for concentration and etch rate. The constant A is generally determined by a flux boundary condition which is unique to the geometry. In the following sections several examples of potentially useful structures will be presented, with solution for both first and second order etch kinetics. Simple geometries are considered first, and are then combined with each other. Constants are summarized in Table 3.

Parameter	Value	[Units]	Reference
D	$1.6\cdot10^{-5}$	[cm^2/sec]	[1,2]
ρ_{SiO2}	2.1	[g/cm^3]	[1,2]
α	4.8	[cm^3/mole]	
C_b	24	[mole/liter]	[3]
k_1	$1.2\cdot10^{-4}$	[cm/mole·sec]	[1,2]
k_2	.065	[cm^4/mole·sec]	[1,2]

Table 3. Constants used for etch model calculations.

3. SIMPLE GEOMETRIES

3.1 Rectilinear etch port open at one end

A schematic of a rectilinear etch channel open at one end with width d, height h, and length L is shown in Figure 1(a). This is the simplest case of an etch structure and is modeled as a one dimensional problem with the longitudinal cross section of Figure 2. For this geometry, the first of Equations 12 is the appropriate form for the concentration. To solve for A, a flux boundary condition from Equation 5 is invoked

$$J_{HF} = -D\left.\frac{\P C}{\P x}\right|_{x=\delta} = -DA \tag{13}$$

Since we are presuming the empirical form $J_{HF}=k_1C+k_2C^2$, Equation 13 becomes

$$-DA = k_1C(\delta) + k_2C(\delta)^2 \tag{14}$$

Substituting $C(\delta)$ rearranging:

$$\left(-\frac{1}{D}k_2\delta^2\right)A^2 + \left(\frac{1}{D}(k_1\delta + k_2\delta^2) - 1\right)A - \frac{1}{D}(k_1C_b + k_2C_b^2) = 0 \tag{15}$$

Solving for A:

$$A = \begin{cases} -\frac{1}{2k_2\delta^2}\left(D + (k_1\delta + k_2C_b)\delta + \sqrt{k_1^2\delta^2 + (2Dk_1 + 4C_bDk_2)\delta + D^2}\right) \\ -\frac{1}{2k_2\delta^2}\left(D + (k_1\delta + k_2C_b)\delta - \sqrt{k_1^2\delta^2 + (2Dk_1 + 4C_bDk_2)\delta + D^2}\right) \end{cases} \tag{16}$$

Only the second root of A satisifies the boundary condition $C(0)=C_b$; the concentration becomes

$$C(x) = \left(-\frac{1}{2k_2\delta^2}\left(D + (k_1\delta + k_2C_b)\delta - \sqrt{k_1^2\delta^2 + (2Dk_1 + 4C_bDk_2)\delta + D^2}\right)\right)x + C_b \tag{17}$$

Usually, it is $C(\delta)$ that is of interest rather than $C(x)$:

$$C(\delta) = \frac{\sqrt{k_1^2\delta^2 + \left(2Dk_1 + 4C_bDk_2\right)\delta + D^2} - D - k_1\delta}{2k_2\delta} \tag{18}$$

The etch rate is given by

$$\begin{aligned} \frac{d\delta}{dt} &= -\alpha DA \\ &= \alpha D\left(\frac{1}{2k_2\delta^2}\left(D + (k_1\delta + 2k_2C_b)\delta - \sqrt{k_1^2\delta^2 + (2Dk_1 + 4C_bDk_2)\delta + D^2}\right)\right) \\ &= \frac{\alpha}{2k_2}\left(\frac{D}{\delta}\right)^2\left(1 + \left(k_1\delta + 2k_2C_b\right)\frac{\delta}{D} - \sqrt{k_1^2\left(\frac{\delta}{D}\right)^2 + \left(2k_1 + 4C_bk_2\right)\frac{\delta}{D} + 1}\right) \end{aligned} \tag{19}$$

It is generally simpler to solve for $t(\delta)$ instead of $\delta(t)$. If Equation 19 is integrated with time going from *0* to t and etch front position going from *0* to δ, $t(\delta)$ becomes

$$t(\delta) = \frac{k_2\left(\frac{D}{k_1^2} - \frac{\delta^2}{D} - \frac{\beta}{k_1^2}\right)\eta - 2\delta - \beta\frac{\delta}{D}}{\alpha\left(k_1^2 - \eta^2\right)} - \frac{k_2D\ln\left(\frac{k_1\beta + k_1^2\delta + \eta D}{D(k_1 + \eta)}\right)}{\alpha k_1^3} \tag{20}$$

$$\eta = k_1 + 2C_bk_2 \qquad \beta = \sqrt{2\eta\delta D + k_1^2\delta^2 + D^2}$$

Equation 20 can be plotted with t on the horizontal axis and δ on the vertical axis, as shown in Figure 5(a). The slope of the curve is the etch rate, which starts at a high value and decreases as the etch progresses. The etch behavior of the port and other simple structures is discussed in more detail in Section **3.4**.

3.2 Bubble solution

The bubble etch is shown in Figure 1(c) and Figure 4. This model can be used for etching any part of a circle from its center. In this model, it is assumed that an infinite supply of etchant is present at r_0 (i.e. at $r=r_0$, $C(r)=C_b$). Therefore the second of Equations 12 is the appropriate form of concentration. Applying a flux boundary condition

$$\begin{aligned} J_{HF} &= -D\left.\frac{\partial C}{\partial r}\right|_{r=\delta} = -D\left.\frac{A}{r}\right|_{r=\delta} = \left.k_1C + k_2C^2\right|_{r=\delta} \\ \Rightarrow\ -D\frac{A}{\delta} &= k_1\left(A\ln\left(\frac{\delta}{r_0}\right) + C_b\right) + k_2\left(A\ln\left(\frac{\delta}{r_0}\right) + C_b\right)^2 \end{aligned} \tag{21}$$

solving for A

$$A = \frac{1}{2\frac{\delta}{D}k_2 \ln\left(\frac{\delta}{r_0}\right)}\left[1 - (k_1 + k_2 C_b)\frac{\delta}{D}\ln\left(\frac{\delta}{r_0}\right) + \sqrt{k_1^2\left(\frac{\delta}{D}\right)^2\ln\left(\frac{\delta}{r_0}\right)^2 + 2\,(k_1 + 2k_2 C_b)\left(\frac{\delta}{D}\right)\ln\left(\frac{\delta}{r_0}\right) + 1}\right] \tag{22}$$

This form of *A* can then be substituted into the second of Equations 12 to obtain the concentration profile

$$C(\delta) = \frac{1}{2\frac{\delta}{D}k_2 \ln\left(\frac{\delta}{r_0}\right)}\left[1 - (k_1 + k_2 C_b)\frac{\delta}{D}\ln\left(\frac{\delta}{r_0}\right) + \sqrt{k_1^2\left(\frac{\delta}{D}\right)^2\ln\left(\frac{\delta}{r_0}\right)^2 + 2\,(k_1 + 2k_2 C_b)\left(\frac{\delta}{D}\right)\ln\left(\frac{\delta}{r_0}\right) + 1}\right] + C_b \tag{23}$$

It is difficult to solve for $t(\delta)$ analytically, but it is given symbolically by

$$t(\delta) = \int_{r_0}^{\delta} \frac{1}{-\left[k_1 C(\delta) + k_2 (C(\delta))^2\right]} d\delta \tag{38}$$

A numerical solution is plotted in Figure 5(b). The etch behavior is discussed in Section **3.4**.

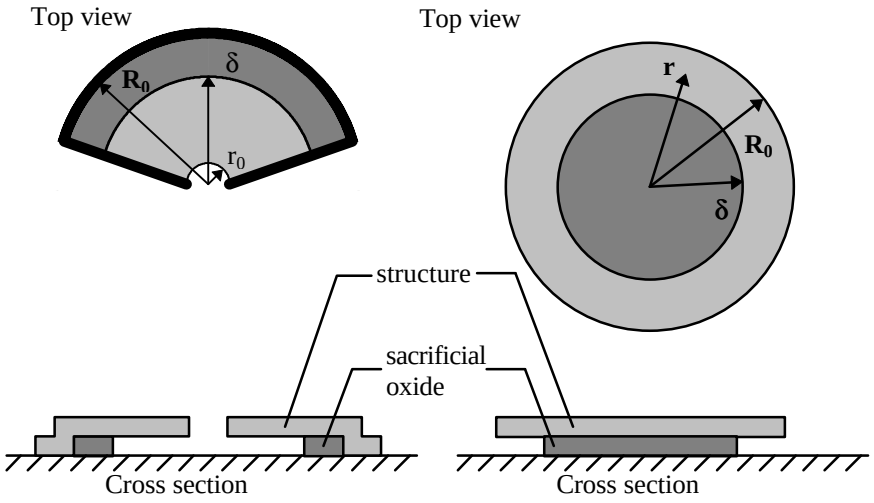

Figure 4. Schematic of bubble (left) and concentric circles (right) etches.

3.3 Concentric circles

Figure 4(right) shows a schematic for etching a circular part from its outside edges. This figure describes a part that will float away after release. A real part would be anchored to the substrate in the middle or at points around the periphery. For this geometry, the supply of etch comes from the edge of the structure, so that $C(R_0)=C_b$. Hence, the second of Equations 12 becomes

$$C(r) = A\ln\left(\frac{r}{R_0}\right) + C_b \tag{25}$$

and the flux can be rewritten as

$$J_{HF} = -D\left.\frac{\partial C}{\partial r}\right|_{r=\delta} = -D\left.\frac{A}{r}\right|_{r=\delta} = -\left.\left(k_1 C + k_2 C^2\right)\right|_{r=\delta} \tag{26}$$

Substituting $C(r)$ from Equation 25, A can be solved

$$A = \frac{1}{2R_0 \left[\ln\left(\frac{d}{R_0}\right)\right]^2} \left[\sqrt{k_1^2 \left(\frac{d}{D}\right)^2 \left[\ln\left(\frac{d}{R_0}\right)\right]^2 - 2h\,\frac{d}{D}\ln\left(\frac{d}{R_0}\right) + 1} - \left(1 - h\,\frac{d}{D}\ln\left(\frac{d}{R_0}\right)\right) \right] \tag{27}$$

Substituting A back into Equation 25 and simplifying yields

$$C(d) = \frac{1}{2R_0 \left[\ln\left(\frac{d}{R_0}\right)\right]^2} \left[\sqrt{k_1^2 \left(\frac{d}{D}\right)^2 \left[\ln\left(\frac{d}{R_0}\right)\right]^2 - 2h\,\frac{d}{D}\ln\left(\frac{d}{R_0}\right) + 1} - \left(1 - h\,\frac{d}{D}\ln\left(\frac{d}{R_0}\right)\right) \right] + C_b \tag{28}$$

An analytical solution for the etch time, $t(d)$, cannot be found. Symbolically, $t(d)$ is given by

$$t(d) = \int_{R_0}^{\delta} \frac{1}{-a\left[k_1 C(d) + k_2 (C(d))^2\right]}\, dd \tag{29}$$

A numerical solution for $t(d)$, transformed so that zero etch distance is at the edge of the structure, is plotted in Figure 5(c).

3.4 Discussion: simple geometries

Each of the simple geometries behaves differently, due largely to changes in the etch front area. For the port solution, the etch front area is considered constant. In the bubble solution, however, the etch front area is continually increasing ~ r^2 . Hence the etch distance vs time rollover in Figure 5 is more pronounced for the bubble solution, since diffusion limitations are more severe. The concentric circles solution faster etch rates. Due to the large perimeter of this geometry, diffusion limitations are not as severe as the port and bubble geometries. Furthermore, the etch starts off fast, slows down, and then speeds up again. The etch front area is continually decreasing for this case. As the etch front area decreases, it requires less HF to propagate the etch. For these kinetics, once the etch front area becomes small enough more HF can be supplied to the etch front and the etch rate increases.

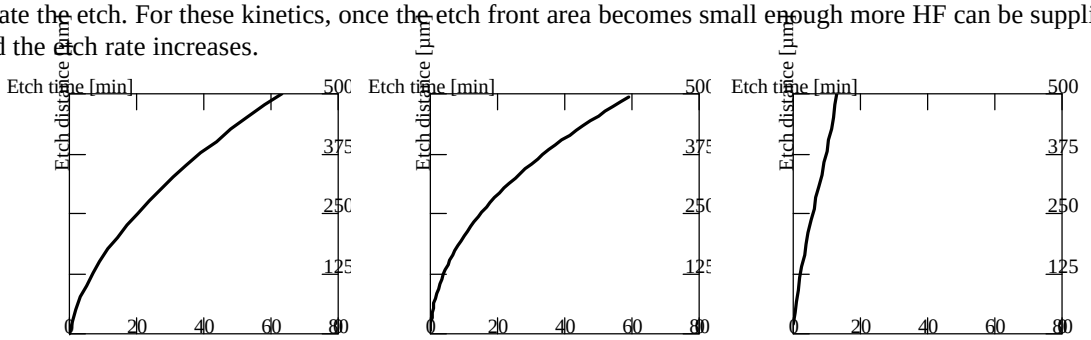

Figure 5. Etch distance vs. Etch time for simple geometries: (a) rectangular etch port, (b) bubble, and (c) concentric circles. The slope of these curves is the instantaneous etch rate.

4. COMPLEX GEOMETRIES

While the preceding simple solutions can be useful on their own, joined solutions enable the modeling of structures that are more likely to be used to make a device. Such is the case for a structure that has small etch ports which lead to a larger chamber. This sort of scheme can be beneficial for creating sealed cavity microstructures[9,10]. By modifying boundary conditions of the simple solutions, a variety of complex structures can be examined.

4.1 Joined ports

The first example is that of two differently sized etch ports, as shown in Figure 1(e), with different widths, d_1 and d_2, heights, h_1 and h_2, and lengths, L_1 and L_2. The subscripts *1* and *2* refer to the region being etched and should not be confused with the subscripts for k_1 and k_2, which denote first or second order etch kinetics. To simplify the mathematics, the origin of the one dimensional coordinate system is initialized to zero for each etching regime.

For etching through the first etch channel the kinetics from Section 3.1 can be used without modification. For etching into the second channel, the solutions are similar. In the concentration equations, C_b is replaced by C_0, which is the concentration at the mouth of the second channel and is a function of d. Hence an additional boundary condition is invoked to solve for C_0 , i.e. $C_2(0) = C_0$ and Equations 18 and 18 are modified to become

$$C_2(x) = \left[-\frac{1}{2k_2\mathrm{d}^2}\left(D + (k_1\mathrm{d} + k_2C_0)\mathrm{d} - \sqrt{k_1^2\mathrm{d}^2 + (2Dk_1 + 4C_0Dk_2)\mathrm{d} + D^2} \right) \right] x + C_0$$

$$C_2(\mathrm{d}) = \frac{\sqrt{k_1^2\mathrm{d}^2 + \left(2Dk_1 + 4C_0Dk_2\right)\mathrm{d} + D^2} - D - k_1\mathrm{d}}{2k_2\mathrm{d}} \tag{30}$$

The function C_0 can be evaluated by applying a total mass flux boundary condtion

$$\left(\textit{Total mass flux}\right)_1 = \left(\textit{Total mass flux}\right)_2 \tag{31}$$

which leads to

$$J_1 \cdot Area_1 = J_2 \cdot Area_2$$

$$\left(-D\frac{\partial C}{\partial x}\right)\Big|_{x = L_1} \cdot (d_1h_1) = \left(-D\frac{\partial C}{\partial x}\right)\Big|_{x = \mathrm{d}} \cdot (d_2h_2) \tag{32}$$

Once etch channel 1 has completed etching, the concentration profile in this channel is presumed to be linear, with one endpoint fixed at C_b and the other at $C_0(\mathrm{d})$ so that Equation 32 becomes

$$\left(\frac{C_0 - C_b}{L_1}\right) d_1h_1 = -\left(-\frac{1}{2k_2\mathrm{d}^2}\left(D + (k_1\mathrm{d} + k_2C_b)\mathrm{d} - \sqrt{k_1^2\mathrm{d}^2 + (2Dk_1 + 4C_bDk_2)\mathrm{d} + D^2} \right)\right) d_2h_2 \tag{33}$$

The linear concentration profile assumption comes from a diffusion model[1]. $C_0(\mathrm{d})$ can now be solved

$$C_0(\mathrm{d}) = \frac{2k_2\mathrm{d}^2C_b - g_p\left[(k_1 - 2k_2C_b)\,\mathrm{d} + k_1g_pD - \sqrt{k_1^2(\mathrm{d} + g_p)^2 + 2D(\mathrm{d} + g_p)(k_1 + 2k_2C_b) + D^2}\right]}{2k_2(\mathrm{d} + g_p)^2} \tag{34}$$

where g_p is given by

$$g_p = \frac{d_2h_2}{d_1h_1}L_1 \tag{35}$$

which leads to the formula for the concentration

$$C_2(\mathrm{d}) = \sqrt{\frac{1}{4}\left(\frac{k_1}{k_2}\right)^2 + \frac{1}{2k_2^2}\left(\frac{D}{\mathrm{d}}\right)\left(k_1 + 2k_2C_0(\mathrm{d})\right) + \frac{1}{4k_2^2}\left(\frac{D}{\mathrm{d}}\right)^2} - \frac{k_1}{2k_2} - \frac{1}{2k_2}\frac{D}{\mathrm{d}} \tag{36}$$

One of the characteristics of the port to port solution is that there is a discontinuity in the concentration between regions 1 and 2. This is a consequence of the one-dimensional nature of the solution, and the resultant etch time accuracy is not expected to be adversely affected. The etch time equation is similar to previous equations, with an additional $t_1(L_1)$ term to assure a continuous $t(\mathrm{d})$. The etch time in the second port, $t_2(\mathrm{d})$ is given symbolically by

$$t_2(\mathrm{d}) = \int_0^{\mathrm{d}} \frac{1}{a\,[k_1C_2(\mathrm{d}) + k_2(C_2(\mathrm{d}))^2]}\,d\mathrm{d} + t_1(L_1) \tag{37}$$

A numerical solution is plotted in Figure 9(a), and the behavior is discussed in more detail in Section **4.5**.

4.2 Port to bubble

The port to bubble solution is shown schematically in Figure 1(d). The solution for $C_2(\mathrm{d})$ is similar to the original bubble solution, except C_b must be replaced by $C_0(\mathrm{d})$, i.e.

$$C_2(d) = \frac{1}{2\frac{d}{D}k_2 \ln\left(\frac{d}{r_0}\right)}\left(-(k_1 + k_2 C_0(d))\frac{d}{D}\ln\left(\frac{d}{r_0}\right) + \sqrt{k_1^2\left(\frac{d}{D}\right)^2\left(\ln\left(\frac{d}{r_0}\right)\right)^2 + 2\,(k_1 + 2k_2 C_0(d))\left(\frac{d}{D}\right)\ln\left(\frac{d}{r_0}\right) + 1}\right) \tag{38}$$

as in the joined ports solution, $C_0(d)$ is solved by a total mass flux boundary condition. The boundary condition is

$$\begin{gathered} J_1 \cdot Area_1 = J_2 \cdot Area_2 \\ \left(-D\frac{\partial C}{\partial x}\right)\Big|_{x = L_1} \cdot (d_1 h_1) = \left(-D\frac{\partial C}{\partial r}\right)\Big|_{r = d} \cdot (\pi d h_2) \\ \left(\frac{C_0 - C_b}{L_1}\right) d_1 h_1 = -\pi h_2 A_2 \end{gathered} \tag{39}$$

A_2 is similar to Equation 22, except C_0 must be substituted for C_b. Making this substitution and solving for C_0 gives

$$C_0(d) = \frac{\left\{2C_b\frac{k_2}{\gamma_b}\frac{d}{D}\left(\ln\left(\frac{d}{r_0}\right)\right)^2 - (k_1 - 2k_2 C_b)\left(\frac{d}{D}\right)\ln\left(\frac{d}{r_0}\right) - \gamma_b k_1\frac{d}{D} - 1 + \sqrt{\left(k_1\frac{d}{D}\ln\left(\frac{d}{r_0}\right) + k_1\gamma_b\left(\frac{d}{D}\right)\right)^2 + 2(k_1 + 2k_2 C_b)\left(\frac{d}{D}\right)\left(\gamma_b + \ln\left(\frac{d}{r_0}\right)\right) + 1}\right\}}{2\gamma_b k_2\frac{d}{D}\left(\ln\left(\frac{d}{r_0}\right)\right)^2 + \frac{1}{\gamma_b}\ln\left(\frac{d}{r_0}\right)^2} \tag{40}$$

where γ_b is given by

$$\gamma_b = \frac{\pi h_2}{d_1 h_1} L_1 \tag{41}$$

The etch time cannot be solved analytically and symbolically is given by

$$t_2(d) = \int_{r_{bp}}^{d} \frac{1}{\left(k_1 C_2(d) + k_2 (C_2(d))^2\right)}\, dd + t_1(L_1) \tag{42}$$

A numerical solution of $t_1(d)$ and $t_2(d)$ is plotted in Figure 9(a). This solution is discussed in Section **4.5**.

4.3 Bubble to wedge

A heretofore unconsidered geometry is now introduced: the wedge. The bubble to wedge solution is useful for characterizing the release etch of a large structure with etch ports on the top (Figure 1(g)). Application of the wet etch model can be used to predict appropriate etch hole spacing. If etch ports are arranged in a square array, then the system can be modeled by considering only one etch port. A close-up of a single etch port is shown in Figure 6. One of the assumptions of this models is that neighboring etch ports can be considered independent of each other, so a single etch port and its surrounding area can be used to describe the etch (Figure 6). The etch starts out in the bubble regime. Then, as all of the bubbles from neighboring etch ports begin to touch, the etch continues in the wedge regime. Furthermore, because of symmetry only one of four corner wedges need be considered to analyze the problem. As etch proceeds in the wedge regime the etch front angle, referenced to the center of the etch port, continually decreases until it becomes zero.

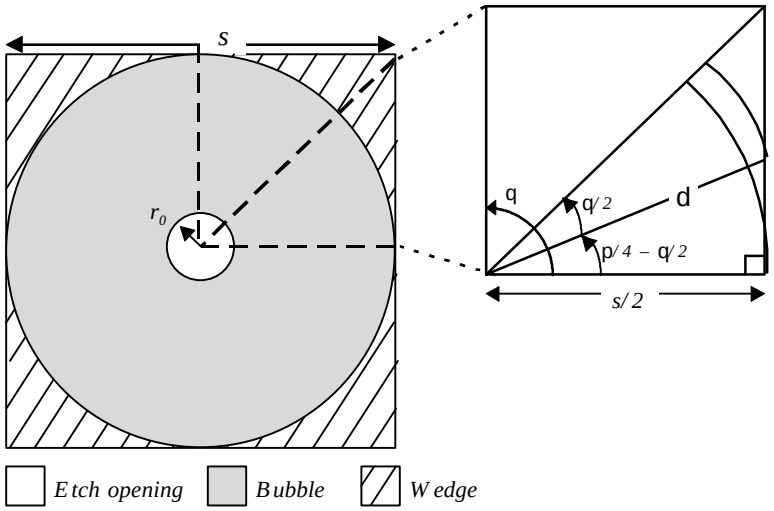

Figure 6. Top view of etching through a single hole. The diagram to the right indicates the conventions for calculating the arc angle θ.

By inspection of the right triangle of Figure 6, the etch angle for the wedge solution is given by

$$\theta = \frac{\pi}{2} - \cos^{-1}\left(\frac{s}{2d}\right) \tag{43}$$

For second order bubble to wedge kinetics the boundary total mass flux boundary is similar to Equation 39

$$\frac{C_b - C_0}{\ln\left(\frac{r_0}{d_{bp}}\right)} = \frac{2\theta(d)}{\pi}\frac{d_{bp}}{d}\frac{1}{2k_2\frac{d}{D}\ln\left(\frac{d}{d_{bp}}\right)}\left(-1 - (k_1 + k_2C_0)\left(\frac{d}{D}\right)\ln\left(\frac{d}{d_{bp}}\right) + \sqrt{1 + k_1^2\left(\frac{d}{D}\right)^2\ln\left(\frac{d}{d_{bp}}\right)^2 + 2(k_1 + k_2C_0)\left(\frac{d}{D}\right)\ln\left(\frac{d}{d_{bp}}\right)}\right) \tag{44}$$

However the slope of the concentration in the initial bubble region has been modified to reflect a logarithmic dependence. It is difficult to solve for $C_0(d)$ algebraically. And hence root functions of common mathematical software packages are recommended. $C_2(d)$ is given by

$$C_2(d) = \frac{-1 - k_1\left(\frac{d}{D}\right)\ln\left(\frac{d}{d_{bp}}\right) + \sqrt{k_1^2\left(\frac{d}{D}\right)^2\ln\left(\frac{d}{d_{bp}}\right)^2 + 2(k_1 + k_2C_0)\left(\frac{d}{D}\right)\ln\left(\frac{d}{d_{bp}}\right) + 1}}{2k_2\frac{d}{D}\ln\left(\frac{d}{d_{bp}}\right)} \tag{45}$$

$C_2(d)$ can be considered a numerical function, hence $t_2(d)$ will also be a numerical function. It is plotted in Figure 9(c), and discussed in Section **4.5**.

4.4 Port to bubble to wedge

The combined port/bubble/wedge solution, which is useful for describing the entire etch process for a circular diaphragm that is etched from its edges through rectangular ports. A schematic of the actual structure and the idealized structure that is used for the model is shown in Figure 7, and a drawing of the port, bubble and wedge regimes is shown in Figure 8. The modeled structure is a regular *n*-sided polygon, where *n* is the number of etch ports. The polygon is circumscribed about the circle, and therefore has a larger area than the circle. Because of symmetry, only a single port is considered. As *n* grows larger, the accuracy of the polygon approximation is expected to improve.

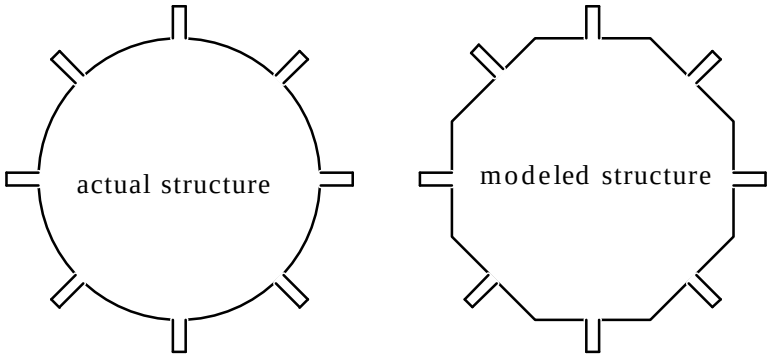

Figure 7. Actual structure (left) of port-to-bubble-to-wedge solution and idealized structure (right) of model.

As a consequence of using a regular *n*-sided polygon for modeling, the etch fronts of the bubble regime are semicircles. The etch progresses through the port and bubble regimes, as in the previous section. When all of the bubbles from neighboring ports are joined, the etch proceeds into the wedge regime. This point in space–time will be referred to as the *break point* (abbreviated by *bp*). One of the important features of the wedge solution is that the area of the etch front continually decreases as the etch progresses. This can be expressed mathematically by constructing an angle θ which is a function of δ. This angle, when multiplied by a radius and oxide height, describes the etch front area. A geometrical construction of this system is shown in Figure 8(right).

For a system with *n* equally spaced ports, the following relationships are true

$$\phi = \frac{2\pi}{n} \qquad \theta_{bp} = 2\phi \qquad \delta_{bp} = R_0 \tan(\phi/2) \qquad R_x = \sqrt{R_0^2 + \delta_{bp}^2} \tag{46}$$

Where ϕ, θ, r, R_0, and R_x are all conventions from Figure 8(right) and the subscript *bp* denotes the space–time point where all of the bubbles have joined. Applying the law of sines to triangle *abe* yields

$$x = \frac{\sin(\theta/2)}{\sin(\phi/2)}\delta \tag{47}$$

and applying the law of sines to triangle *bce* yields

$$\frac{\sin(\pi/2 - \theta/2)}{R_x - x} = \frac{\sin(\pi/2 - \phi/2)}{\delta} \tag{48}$$

By removing *x* from the above two equations, a form for $\theta(\delta)$ can be found

$$\theta(\delta) = 4\tan^{-1}\left(\frac{\delta\cos\left(\frac{\phi}{2}\right) - \sqrt{\delta^2 - \frac{\sin^2(\phi)}{4}\left(R_0^2 + \delta_{bp}^2\right)}}{\sin\left(\frac{\phi}{2}\right)\left(\delta + \cos\left(\frac{\phi}{2}\right)\sqrt{R_0^2 + \delta_{bp}^2}\right)}\right) \tag{49}$$

$\theta(\delta)$ tends to zero as δ tends to R_0, which coincides with the complete consumption of the oxide.

Boundary conditions for this problem are $C(r_0) = C_0$ and $C(\delta_{bp}) = C_w$. and the total mass flux is balanced over the three regimes

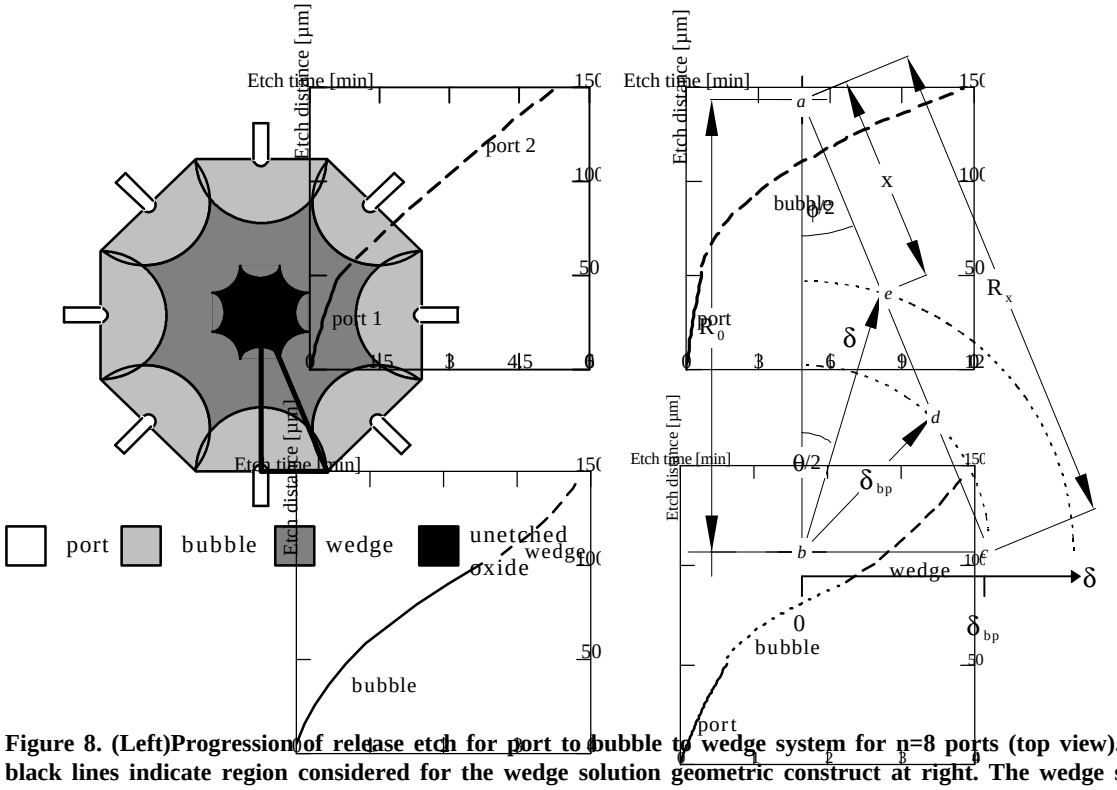

Figure 8. (Left)Progression of release etch for port to bubble to wedge system for n=8 ports (top view). Heavy black lines indicate region considered for the wedge solution geometric construct at right. The wedge solution begins after all of the bubbles from neighboring etch ports are joined. (Right) Geometric construct of wedge solution. Half of a wedge being fed by an etch port is shown. Dimensions are accurate for *n=8*.

Figure 9. Etch time vs Etch distance for complex solutions: (a) port to port, (b) port to bubble, (c) bubble to wedge, and (d) port to bubble to wedge. Geometric parameters are: $h_1=h_2=1$ μm. $d_1=10$μm, $d_2=50$ μm, $L_1=50$ μm, $L_2=100$μm, $R_0=100$ μm, s = 100 μm (bubble to wedge).

$$
\begin{aligned}
d_1 h_1 \left(J_{port} \right) &= \pi r h_2 \left(J_{bubble} \right) = \theta r h_2 \left(J_{wedge} \right) \\
d_1 h_1 \left(-D \frac{\partial C_1}{\partial x} \right) &= \pi r h_2 \left(-D \frac{\partial C_2}{\partial r} \right) = (r\theta) h_2 \left(-D \frac{\partial C_3}{\partial r} \right) \\
d_1 h_1 \left(\frac{C_0 - C_b}{L_1} \right) &= \pi r h_2 \left(\frac{1}{r} \frac{C_w - C_0}{\ln(\delta_{bp}/r_0)} \right)_{r=\delta_{bp}} = (r\theta) h_2 \left(\frac{A}{r} \right)_{r=\delta_{bp}}
\end{aligned}
\tag{50}
$$

By using the left two of these equations the following relationship is derived

$$
C_0(\delta) = \frac{C_b \ln\left(\frac{\delta_{bp}}{r_0}\right) + \gamma_b C_w}{\ln\left(\frac{\delta_{bp}}{r_0}\right) + \gamma_b}
\tag{51}
$$

This form of C_0 can be substituted into the right two equations to solve for C_w. However, since A_3 is similar to Equation 22 of the bubble solution, it is quite complicated, and C_w is generally solved numerically. A_3 and C_3 are given by

$$
\begin{aligned}
A_3 &= \frac{1}{2k_2 \frac{\delta}{D} \ln\left(\frac{\delta}{\delta_{bp}}\right)} \left(\sqrt{k_1^2 \left(\frac{\delta}{D}\right)^2 \ln^2\left(\frac{\delta}{\delta_{bp}}\right) + \left(2k_1 + 4k_2 C_w \right) \frac{\delta}{D} \ln\left(\frac{\delta}{\delta_{bp}}\right)} - (k_1 + 2k_2 C_w) \frac{\delta}{D} \ln\left(\frac{\delta}{\delta_{bp}}\right) - 1 \right) \\
C_3(\delta) &= A_3 \ln(\delta, \delta_{bp}) + C_w
\end{aligned}
\tag{52}
$$

$C_w(\delta)$ is solved numerically. The numerical solutions for the etch time is plotted in Figure 9(d).

4.5 Discussion: complex geometries

The port to port solution, although having a discontinuous slope change, behaves as expected. Once the etch proceeds from the first port to the second port, the etch front area is rapidly increased and requires more etchant, hence increasing diffusion limitations and decreasing the etch rate. The port to bubble solution has a smoother transition and the etch rate in the bubble regime rapidly decreases below the etch rate of the port to port solution, due to a continuously decreasing etch front area. The combined bubble to wedge etch rate starts high, decreases, and then accelerates at the end. Again, this acceleration is due to the rapidly diminishing etch front area of the wedge. The final solution, the port to bubble to wedge also shows behavior similar to the concentric circles solution, however the etch rate flattens out much more in this solution, due to the diffusion resistance of the etch port. It should be noted that all of the etch cases in Figure 9 have the same total etch length, the etch times are very different.

The port to bubble to wedge solution is a good example of the importance of etch rate modeling. Etch rates inferred from etching in the port regime would be drastically underestimated, whereas the converse would be true for etch rates inferred from the bubble regime. Only by understanding the entire etch process can accurate etch times be predicted.

5. ACKNOWLEDGEMENTS

This work was performed and supported at Sandia National Laboratories by the U.S. Department of Energy under contract DE-AC04-94AL85000

Special thanks to the staff and operators of Sandia National Laboratories' Microelectronics Development Laboratory, without whom the devices could not have been made.

6. REFERENCES

1 J. Liu, Y.-C. Tai, J. Lee, K.-C. Pong, Y. Zohar, and C.-H. Ho, "*In Situ* monitoring and universal modeling of sacrificial PSG etching using hydrofluoric acid", *Proceedings of Micro Electro Mechanical Systems, IEEE,* pp. 71-76 (February 1993).

2 Y.-C. Tai and C.-M. Ho, "Silicon Micromachining and Its Applications", *Proceedings of the SPIE, Smart Structures and Materials 1995: Smart Electronics,* **Vol 2448**, pp. 141-151 (March 1995).

3 D.J. Monk, "Controlled Structure Release for Silicon Surface Micromachining", *Ph.D. Dissertation, University of California at Berkeley*, Department of Chemical Engineering (1993).

4 D.J. Monk, D. S. Soane, and R.T. Howe, "Determination of the etching kinetics for the hydrofluoric acid/silicon dioxide system," *Journal of the Electrochemical Society*, **140**(8), pp. 2339-2346(Aug. 1993).

5 D.J. Monk, D. S. Soane, and R.T. Howe, "Hydrofluoric acid etching of silicon dioxide sacrificial layers, part II. Modeling," *Journal of the Electrochemical Society*, **141**(1), pp. 270-274 (Jan. 1994).

6 Mathematica, Wolfram Research, Inc, 100 Trade Center Drive, Champaign, IL 61820-7237.

7 Maple V, Waterloo Maple Inc.,450 Phillip Street, Waterloo, Ontario Canada N2L 5J2.

8 MathCAD, MathSoft, Inc., 101 Main Street, Cambridge, MA 02142-1521.

9 D.W. Burns, "Micromechanics of Integrated Sensors and the Planar Processed Pressure Transducer", *Ph.D. Dissertation, the University of Wisconsin-Madison*, (May 1988).

10 H. Guckel, and D.W. Burns, "Planar Processed Polysilicon Sealed Cavities for Pressure Transducer Arrays", *Technical Digest: IEEE International Electron Devices Meeting, IEDM '86*, pp. 223-225 (1984).